NASA/TM–20260002019

Hybrid Modeling Study on Grain Evolution in the Metal Welding Process and Its Potential Lunar Application

Wei Li
The University of Texas at Dallas, Richardson, Texas

Fredrick N. Michael
Marshall Space Flight Center, Huntsville, Alabama

NASA STI Program Report Series

Hybrid Modeling Study on Grain Evolution in the Metal Welding Process and Its Potential Lunar Application

Wei Li
The University of Texas at Dallas, Richardson, Texas

Fredrick N. Michael
Marshall Space Flight Center, Huntsville, Alabama

March 2026

Available from:

NASA STI Program / Mail Stop 050
NASA Langley Research Center
Hampton, VA 23681-2199

Table of Contents

Abstract

Metal is most commonly used structural material in a wide range of spacecraft, and welding is the principal method for joining metal components into functional systems. However, conducting welding experiments under extreme environments—such as microgravity or vacuum conditions in space—is prohibitively expensive and experimentally challenging. To overcome these limitations, multi-physics computational welding models provide a cost-effective and versatile alternative. In this work, the authors have developed a coupled thermal (fluid) microstructure simulation framework to model metal welding under varying gravity conditions. The framework integrates a mixed-mode heat transfer formulation (conduction, convection, and radiation) with molten pool fluid dynamics, enabling accurate prediction of temperature fields and weld-pool geometry. A grain growth model is further incorporated to capture the spatial and temporal evolution of microstructure, including grain size distribution and morphological transitions during solidification. This approach provides detailed insight into molten pool evolution and grain-level microstructure development throughout the welding process. By explicitly parameterizing environmental conditions, the model supports extrapolation to off-Earth manufacturing scenarios such as welding on the lunar surface. Tantalum—chosen in this study due to its high melting point, oxidation resistance, and mechanical stability at elevated temperatures—serves as the material system for model demonstration. Beyond Tantalum, the integrated multi-physics framework offers broad applicability for predictive welding simulations of various structural and refractory metals or alloys used in extreme terrestrial or extraterrestrial environments.

Keywords: Welding model; thermos-fluid model; Kinetic Monte Carlo Potts model; microstructure evolution.

1.0 Introduction

Welding remains one of the most widely employed techniques for joining metallic components, and the physical properties of the resulting joints are critical to their engineering performance. This process involves the application of a localized heat source to melt adjoining regions of two parts, enabling fusion upon cooling and solidification. As the heat source traverses along the joint, a molten pool forms ahead while the trailing region undergoes cooling, solidification, and microstructural evolution. This dynamic thermal environment gives rise to weld microstructures that are distinct from those produced by conventional solidification processes. In particular, welds often exhibit elongated and curved columnar grains—arising from the interplay of heat flow, solidification front velocity, and crystallographic growth orientations. Since grain size, morphology, and orientation strongly influence the mechanical, thermal, and corrosion properties of welds, predictive understanding of microstructural development is essential for engineering joints with tailored performance.

Metal is the primary structural material in various aerospace crafts, and some metals with special properties are widely used in the aerospace field. Tantalum is a critical strategic metal widely employed in aerospace structural components due to its high melting point, excellent oxidation resistance, and mechanical stability under extreme thermal and mechanical loads. Welding remains the principal method for fabricating Tantalum-based assemblies; however, the rarity and high cost of Tantalum severely limit experimental investigations into its joining behavior. Furthermore, the extreme conditions under which Tantalum welds, which are expected to operate in fields ranging from high-temperature aerospace propulsion systems to potential extraterrestrial environments, introduce additional complexities that are challenging to replicate experimentally. As a result, multi-physics modeling and simulation offer an effective alternative for studying the thermal, fluid flow, and microstructural evolution during Tantalum welding. Such approaches enable systematic exploration of weld pool dynamics, heat transfer, and grain growth mechanisms under varied environmental conditions, while substantially reducing material costs. Beyond terrestrial applications, predictive modeling also provides a pathway to assess weldability and microstructural stability of Tantalum components in space-relevant environments, such as low-gravity conditions on the lunar surface.

In this work, the authors present a computational framework capable of simulating heat transfer and molten pool evolution, as well as grain growth during welding. The model incorporates coupled heat transfer, fluid flow, and microstructural kinetics to capture the transient evolution of the molten pool and grain-level microstructure. Such predictive modeling provides a valuable tool for designing welding processes to achieve microstructures optimized for strength, toughness, and long-term service reliability under demanding lunar environments (as shown in Fig.1).

Figure.1. In-space metal welding operation on the Moon.

2.0 Modeling Approach: Hybrid Thermo-Fluid and KMC Potts Model

2.1 Thermal-Fluid Model

The authors established a thermal-fluid model (as shown in Fig. 2) to simulate the interaction between laser beam and metal substrate, evolution of molten pool, phase change, and transient temperature fields over the entire metal substrate. The thermal-fluid model is essential to computationally measure the important laser welding physical quantities such as temperature gradients, cooling rates, and molten pool geometry that affect the microstructure of the welded parts. Close to the simulation domain of molten pool, the thermal-fluid model needs to run in small scale with fine meshes to simulate the molten pool evolution. Moreover, the time increment used for explicit integration has to be correspondingly reduced [1].

The thermal fluid in the molten pool commonly follows the conservation equations of mass, momentum, and energy in transient form (Eq. 1−3) [1−3], where $\vec{v}$ is the velocity of molten pool, *t* is the time, *p* indicates the pressure, ρ is the density, μ is the average viscosity in liquid metal, $\vec{g}$ is the gravity, F_b is the body force sources in the system, $\dot{q}$ is the Gaussian heat source of laser beam, *h* is the enthalpy, *k* is the thermal conductivity, and *T* is the temperature [2].

$$\nabla \cdot \vec{v} = 0 \tag{1}$$

$$\frac{\partial \vec{v}}{\partial t} + (\vec{v} \cdot \nabla)\vec{v} = -\frac{1}{\rho}\nabla P + \mu \nabla^2 \vec{v} + \vec{g} + F_b \tag{2}$$

$$\frac{\partial h}{\partial t} + (\vec{v} \cdot \nabla)h = -\frac{1}{\rho}(\nabla \cdot k\nabla T) + \dot{q} \tag{3}$$

The phase change between liquid phase and solid phase is simulated with the consideration of latent heat [2, 3]. When the metal temperature is between solidus and liquidus temperatures, an additional energy term is added to enthalpy. The enthalpy term is updated in Eqs. 4−6. The variable *f* is the volumetric fraction of liquid determined by temperature. C_p is the material-specific heat. L_f is latent heat of fusion. T_s and T_L are metal's solidus and liquidus temperatures, respectively [3]. In addition, the volume of fluid (VOF) method will be used to track the instant free surface evolution of the molten pool [4]. In the VOF method (in Eq. 6), *F* is defined as the fluid volume fraction ($0 \leq F \leq 1$). An empty cell (no fluid) is defined as *F*=0 while a cell fully filled with fluid is defined as *F*=1. If a cell is partially fluid and partially void, F is defined as $0<F<1$.

$$h = C_p \cdot T + f(T) \cdot L_f \tag{4}$$

$$f = \begin{cases} 0, & T < T_s \\ \frac{T - T_s}{T_L - T_s}, & T_s \leq T \leq T_L \\ 1, & T > T_L \end{cases} \tag{5}$$

$$\frac{\partial F}{\partial t} + \nabla \cdot (\vec{v}F) = 0 \tag{6}$$

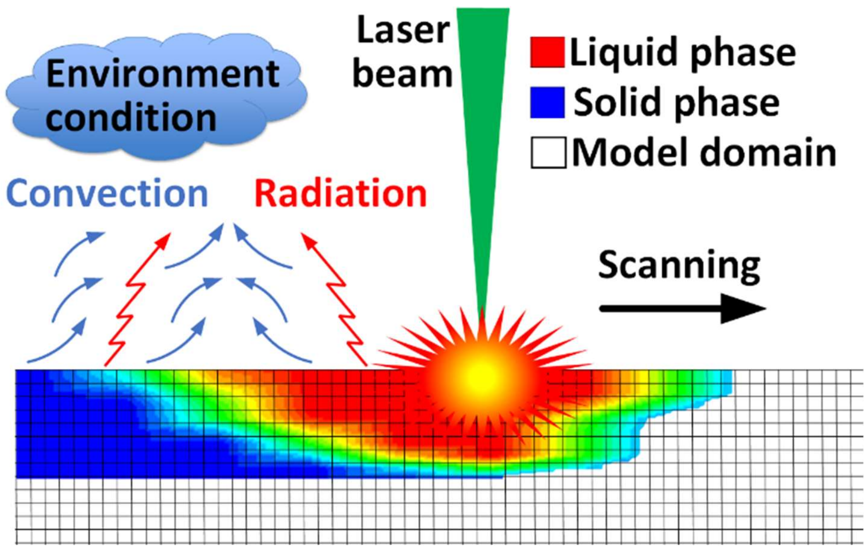

Figure 2. Simulating welding process with thermo-fluid model.

2.2 Grain Evolution Model

The authors built a grain evolution model with the KMC-Potts approach to simulate the microstructure in the welded part. The KMC-Potts model assigns an integer index to a cluster of continuum lattice sites, which indicates a grain. All the sites within a grain have the same index. As shown in Figure 3, the interfaces between nearest neighboring sites with different indices are used to indicate grain boundaries [5−7]. The principle of curvature-driven grain growth during the solidification process is minimizing grain boundary energy. The KMC-Potts model calculates the grain boundary energy by the sum of the bond energy between neighboring lattice sites with different indices [8−10] in Eq. 7, where N is the total number of lattice sites; q_i and q_j are the index at the grain lattice sites i and j; and L is the number of neighbors of each grain lattice site. A factor of 0.5 is applied to eliminate double-counting in the summation [8, 10]. One energy unit is contributed by each pair of different neighboring sites to the total system energy according to the above equation. The simulation of grain growth starts with reassigning a lattice site's index to a different neighboring site at random. This step causes a change in the overall system energy. The total energy of the system is recalculated with Eq. 7. The grain growth will happen if the index reassignment is accepted; otherwise, if the index reassignment is rejected, the grain growth will not happen. The probability of accepting the index reassignment is determined by the Metropolis function in Eq. 8 [8], where ΔE is the system energy change; k_B is Boltzmann's constant; and T_s is the local site temperature. The index reassignment is successful if the energy change is less than zero, which means there is a decrease in system energy, and grain growth will happen. If the energy change is positive, the probability of grain growth or grain boundary migration will follow the Boltzmann distribution.

$$E = \frac{1}{2}\sum_{i=1}^{N}\sum_{j=1}^{L}\left(1 - \delta\left(q_i, q_j\right)\right) \tag{7}$$

$$P = \begin{cases} exp\left(\frac{-\Delta E}{k_B T_s}\right) & if\ \Delta E > 0 \\ 1 & if \Delta E \leq 0 \end{cases} \tag{8}$$

$$M = M_0\, exp\left(\frac{-Q}{RT(t,i)}\right) \tag{9}$$

$$P = \begin{cases} M * \exp\left(\frac{-\Delta E}{k_B T_s}\right) & if\ \Delta E > 0 \\ M & if \Delta E \leq 0 \end{cases} \tag{10}$$

During the welding process, metallic substrate is locally melted by laser beam and forms a molten zone. Meanwhile, because of heat transfer from the molten zone to the surrounding material, a heat-affected zone (HAZ) [11−13] with a steep thermal gradient is generated. The grain evolvement is concurrently controlled by the mobilities of both the molten zone and the HAZ. In order to simulate this process, some adaptations were made to the above KMC-Potts model. A grain boundary mobility with the local temperature is defined in Eq. 9 [8], where constant Q is the activation energy for grain boundary motion; M_0 is the Arrhenius pre-factor; R is the gas constant; and $T(t,i)$ is the local temperature with time t and location i. Then the probability of accepting the index reassignment for grain evolvement in the welding process is updated in Eq. 10 [8, 9]. Figure 3-d shows a mechanism of grain evolvement in welding process simulated with KMC-Potts model. A top view of the grain evolution with the molten pool and solidification boundary is schematically illustrated. As the molten pool moves forward, the trailing area solidifies and then temperature gradient causes grains to grow quickly. According to the KMC-Potts model, grains grow by doing Monte Carlo switches with unlike indices of neighboring grains. Index reassignment can happen with indices of formerly solidified grains (causing grain growth) or among lattice sites that just exited the molten pool (causing grain nucleation).

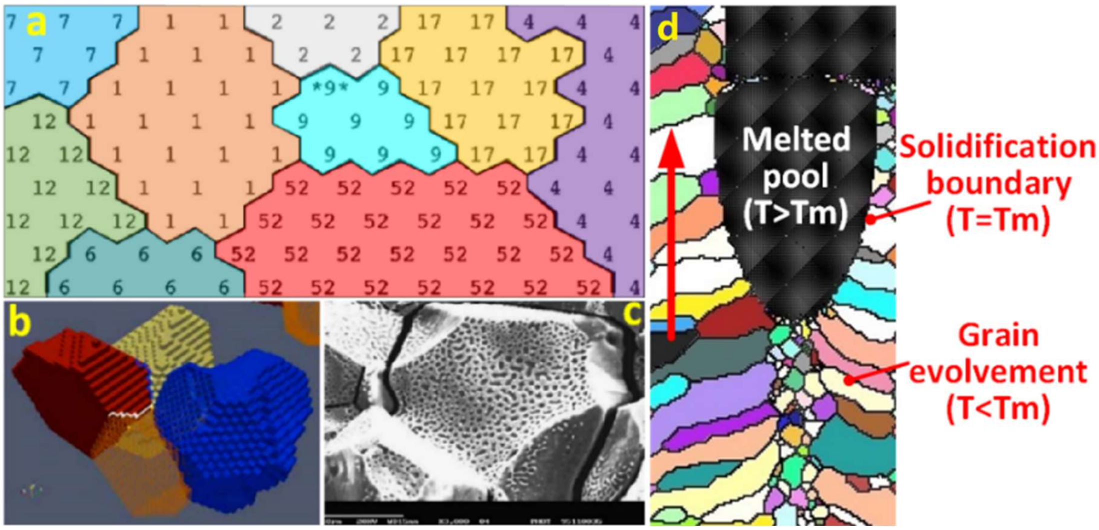

Figure 3. Grain and boundary in KMC-Potts: (a) 2-D view; (b) 3-D view; (c) real grains; and (d) mobility function in the KMC-Potts model.

2.3 Simulation Domain and Modeling Conditions

The thermal-fluid model was solved using a commercially available Flow3D CFD solver. The domain was set with a grid size of 50 microns (Fig. 4). The substrate was modeled inside the domain as a solid rectangle with fluid steel properties set, assuming this is a solid region. The rest of the domain was modeled as an air region. The gravity conditions in the model were set up according to the terrestrial condition (9.81 m/s^2 gravity) and lunar condition (1.62 m/s^2 gravity). The modeled environmental conditions can be adjusted into other planets such as the Mars.

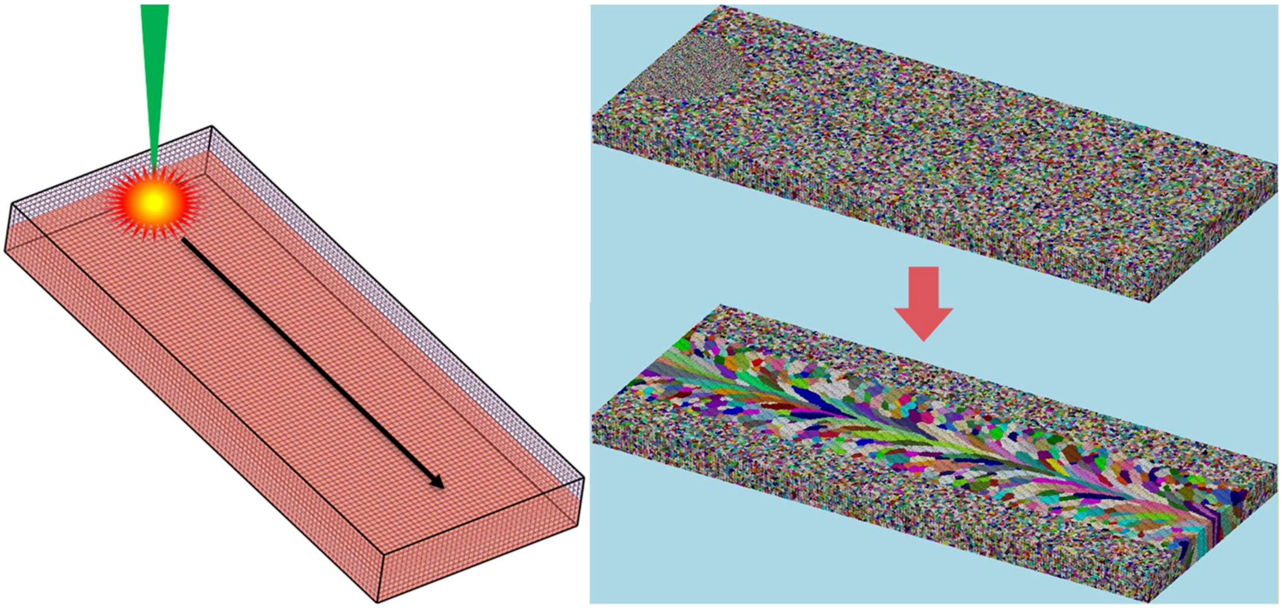

Figure 4. Simulation domain for performing the thermos-fluid model.

3.0 Simulation Results and Analysis

3.1

During the welding process modeled in both terrestrial and lunar environments, three representative time steps (t=0.2s, t=1.0s, t=1.8s) were selected to capture the temporal evolution of the molten pool. Figure 5 illustrates the pool morphology from three perspectives: view of temperature distribution, view of molten pool shape, and view of grain morphology. At each time step, the molten pool geometry reflects the dynamic balance between heat input from the moving source and heat dissipation. The pool boundary was defined as the region where the local temperature exceeded the melting point of metal, thereby delineating the fusion zone. The thermal history and molten pool morphology can govern the local solidification dynamics. Regions with steep temperature gradients at the pool boundary favor the formation of columnar grains aligned with the welding direction, while areas with reduced gradients near the trailing edge promote equiaxed nucleation. By transferring the molten pool boundary information from the thermo-fluid model into the KMC-Potts model, the simulations capture this interplay, enabling quantitative predictions of grain growth and grain morphology within the weld joint. These results provide critical insights into how process parameters—such as laser power, beam size, travel speed, and gravity—directly influence microstructural evolution of the metallic welds, thereby tailoring microstructural features through control of process parameters, informing the design of welding strategies that optimize the performance of welding joints in aerospace applications

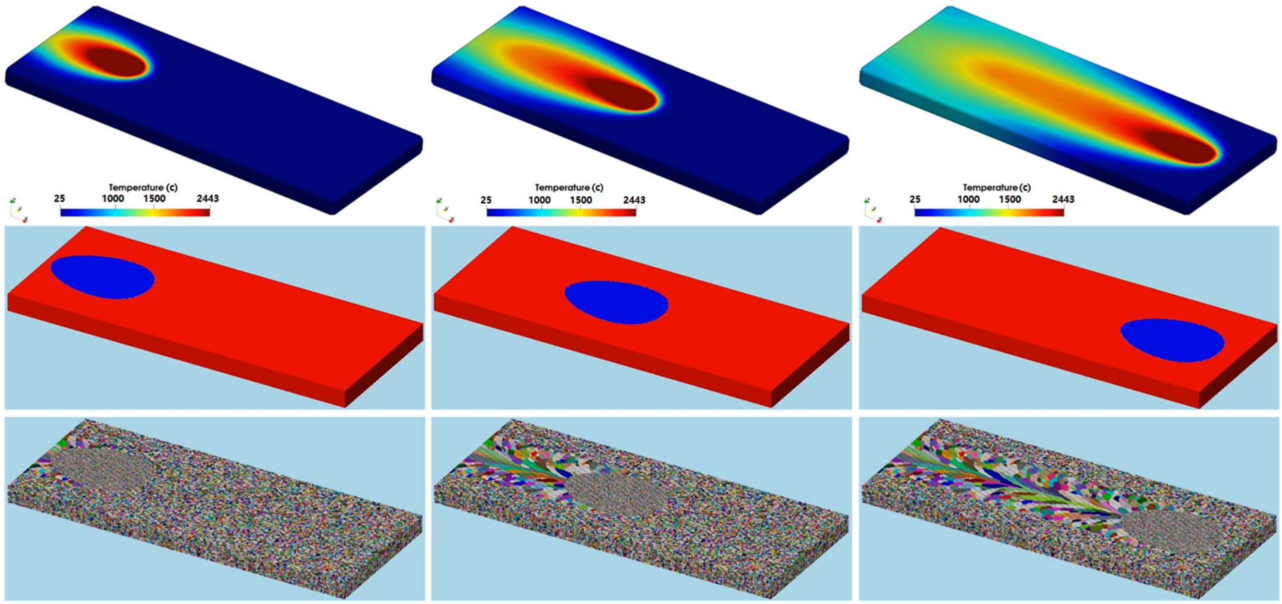

(a)

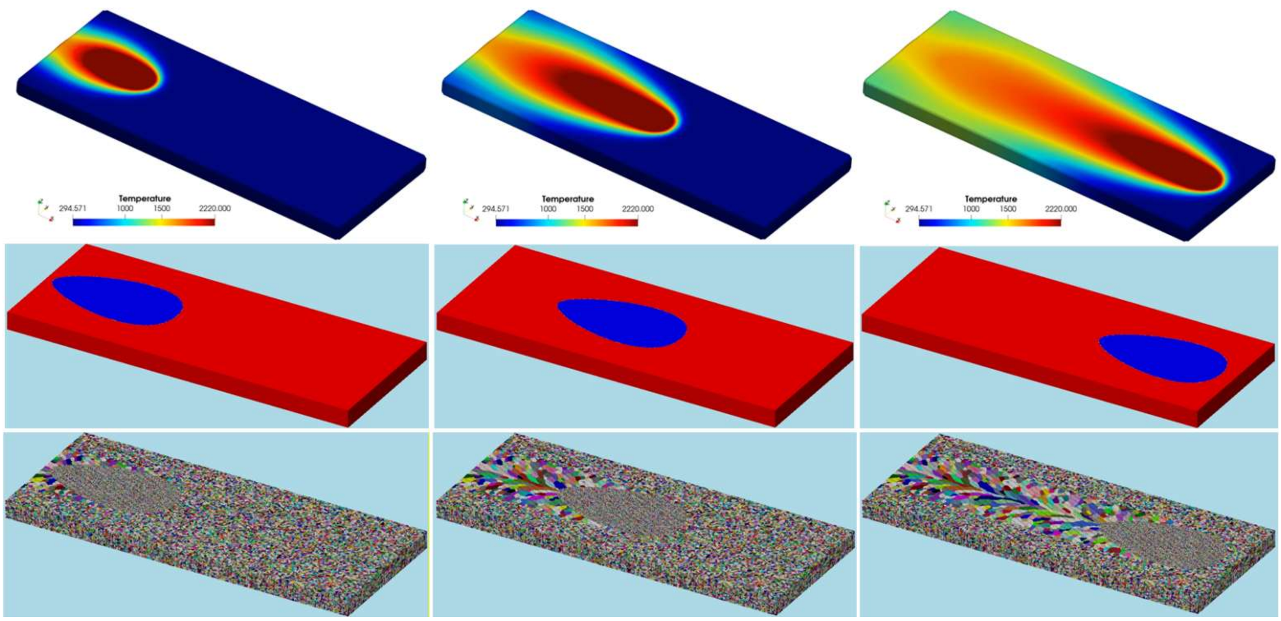

(b)

Figure 5. Temperature history, molten pool evolution, and grain evolution at three time steps (t=0.2s, t=1.0s, t=1.8s) in both (a) terrestrial and (b) lunar environments.

3.2 Molten Pool Boundary in Welding

The molten pool boundaries extracted from the thermo-fluid model were subsequently used as input to calculate the local surface energy distribution at the solid-liquid interface. This information served as the basis for simulating grain growth during the welding process. Figure 5 presents the molten pool geometries obtained at three representative time steps, highlighting the temporal evolution of the fusion zone. Using these geometries as reference domains, the KMC-Potts model was employed to simulate the progression of grain growth.

3.3 Description of Predicted Grain Evolution

To further examine the evolution of grain morphology during the welding process, both top-view and side-sectional microstructures of the welding joint are presented in Figure 6. The results indicate that the weld zone is dominated by columnar grains, which constitute the primary microstructural feature. This prevalence arises from the rapid solidification and steep thermal gradients inherent to the welding process, which drive grain growth preferentially along the direction of laser scanning. Consequently, grains in the fusion zone exhibit elongated, stretched morphologies aligned with the trailing movement of the molten pool. This columnar tendency is particularly evident in the side-sectional view, where the anisotropic grain growth can be clearly observed.

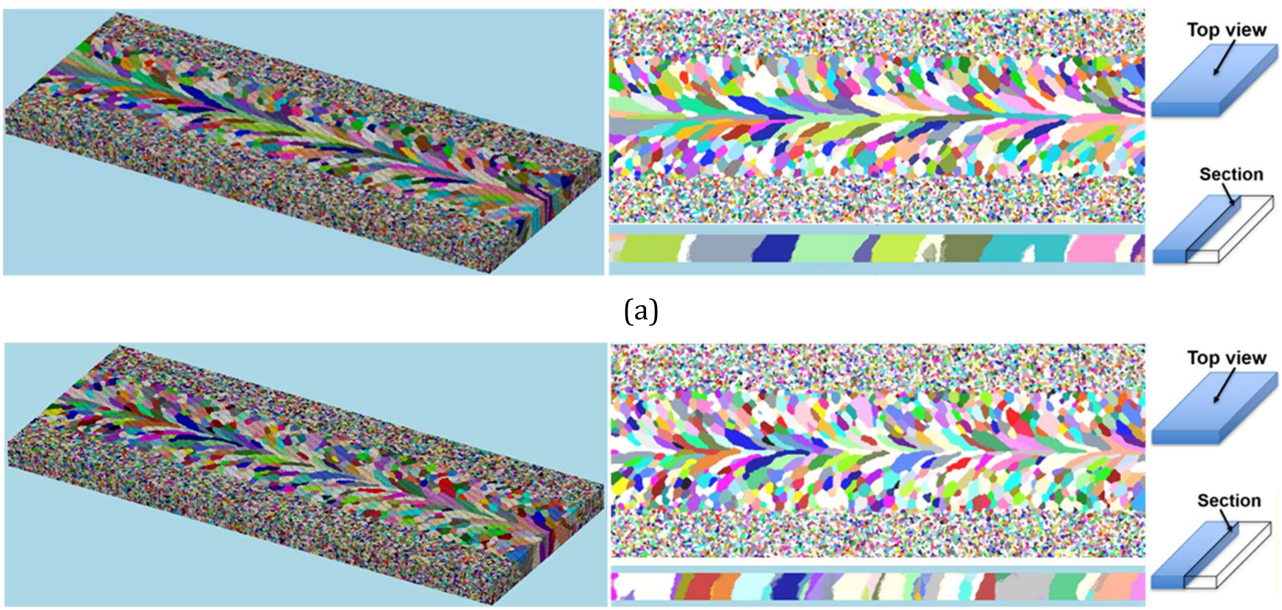

(b)

Figure 6. Grain morphology after welding; top view and cross-section side view of the grains simulated in both (a) terrestrial and (b) lunar environments.

In contrast, regions away from the molten pool, where the thermal gradients are reduced and cooling rates are less severe, show a predominance of equiaxed grains. These grains nucleate under conditions of higher undercooling and more isotropic thermal fields, leading to a more randomized grain orientation. The coexistence of columnar and equiaxed structures highlights the strong coupling between local thermal conditions and microstructural evolution. Such insights provide important implications for tailoring the weld microstructure of metallic joints by controlling welding parameters to balance columnar and equiaxed grain formation, thereby optimizing the mechanical performance of welded components.

Figure 7 is used to describe the grain evolutions at three time steps, t=0.2s, t=1.0s, and t=1.8s. The authors selected top view and cross-section views to show the grain morphologies simulated under terrestrial and lunar environments. Due to the distinct thermal distributions and histories of the molten pool, the grain morphologies that develop along the welding path differ significantly between terrestrial and lunar welding conditions. Variations in gravity and heat dissipation produce welding process changes on solidification behavior, leading to different grain sizes, shapes, and orientations. These differences are evident in both the top-view and side-view grain-level microstructural sections, each revealing unique features of the grain morphology that arise from the contrasting environmental conditions.

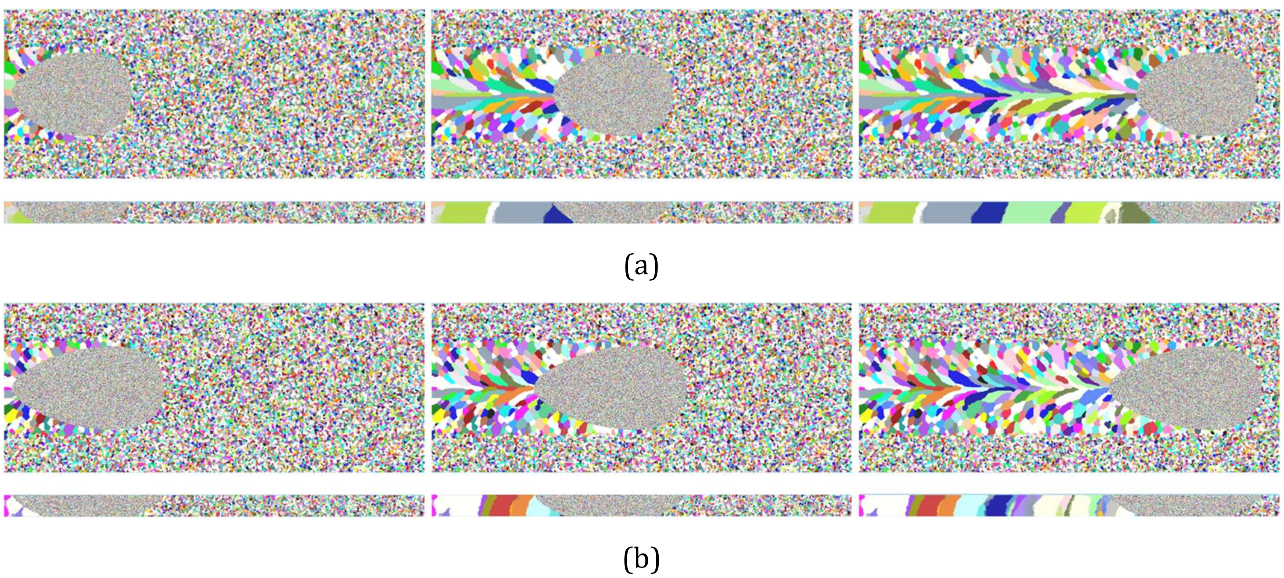

Figure 7. Grain morphology (top view and cross-section side view) at three time steps (t=0.2s, t=1.0s, and t=1.8s) simulated in both (a) terrestrial and (b) lunar environments.

Furthermore, the simulated grain morphology of the welded joint exhibits good agreement with experimentally observed microstructures reported for Tantalum welds (Fig.8). This consistency between simulation and experiment provides a robust validation of the developed multi-physics modeling framework, confirming its capability to reliably capture the coupled thermal, fluid, and microstructural phenomena governing weld.

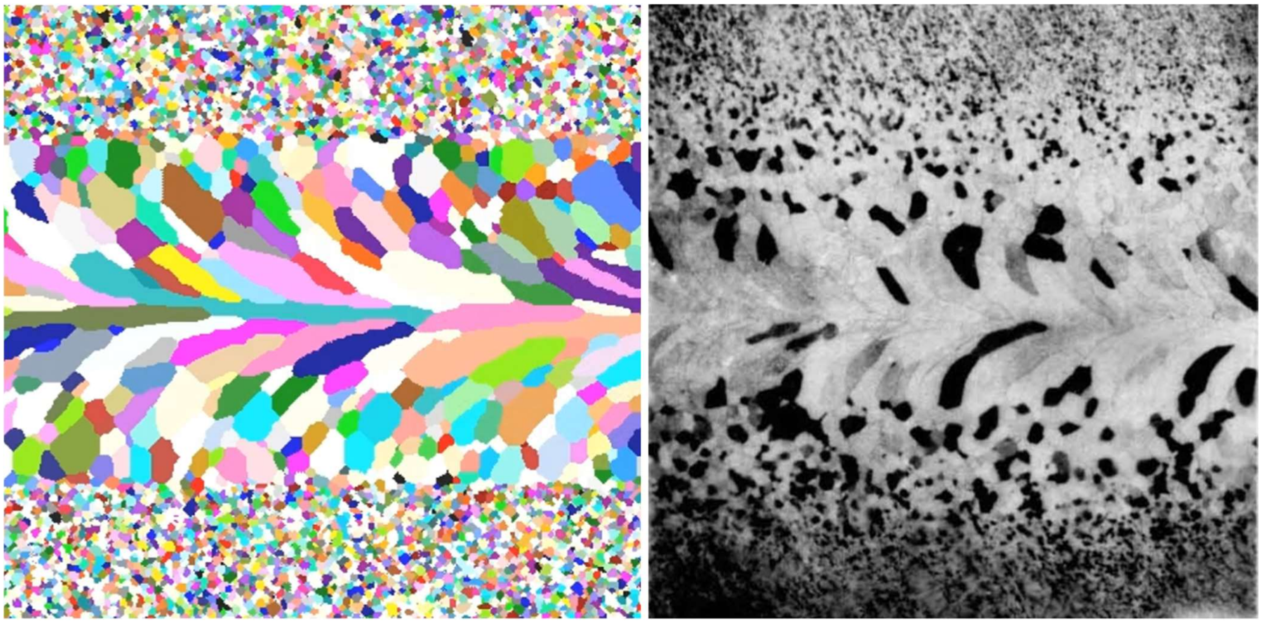

Figure 8. Comparison of simulated grain morphology and experimentally observed grain morphology in the welding joint [14].

3.2 Quantifying the Simulated Grain Morphologies

It is necessary to quantify the distinctive grain morphology generated in the welding process. In this study, the Image J software [15] was used to quantify the grain morphologies in the simulation results. Three quantification parameters were considered: aspect ratio, grain orientation, and grain size. Illustrations of grain quantification are introduced in Figure 9. An ellipse is applied to best-fit a grain. The aspect ratio of the grain is the ratio of the ellipse's minor axis and major axis [15]. The aspect ratio of the grain is a number ranging between zero and one. If aspect ratio is close to zero, this means the grain cross-section is near circular. If aspect ratio is closer to one, this means the grain cross-section has a needle-like shape. The grain orientation is the angle of the major axis in best-fit ellipse. Grain size is the dimension of major axis of fit ellipse [16].

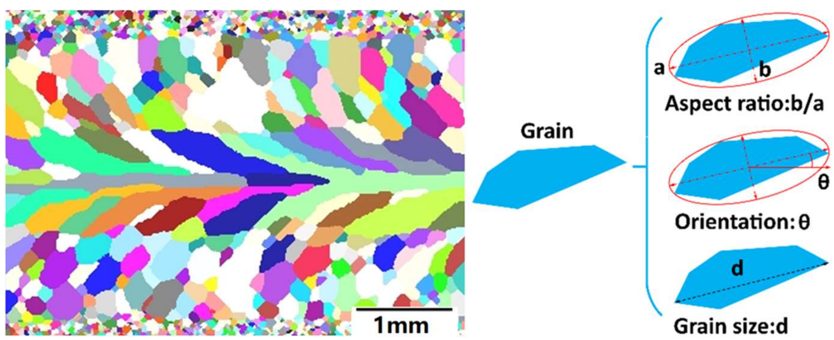

Figure 9. Quantifying the grain morphology: aspect ratio, grain direction, and grain size.

Figure 10 presents the statistical distributions of grain morphology and directions within the welded joint. The aspect ratio distribution shows two primary peaks near 0.3 and 1.0, corresponding to columnar and equiaxed grains, respectively. This indicates that both solidification modes co-exist within the weld microstructure: equiaxed grains dominate the regions farther from the fusion boundary, while columnar grains prevail in the vicinity of the molten pool due to strong directional solidification. The grain orientation distribution in the top view further reveals two distinct peaks, reflecting the preferred alignment of columnar grains along directions consistent with the thermal gradient. Since grain growth tends to follow the steepest cooling direction during solidification, the observed bi-modal orientation distribution is consistent with the evolution of the moving heat source and the asymmetric cooling conditions in the weld pool. Besides the grain aspect ratio and grain orientation, another important indicator is grain size, which can quantitatively describe the size of microstructural morphology. By comparing the welding grain morphologies under the two gravitational conditions, both the grain aspect ratio and the grain direction are very close.

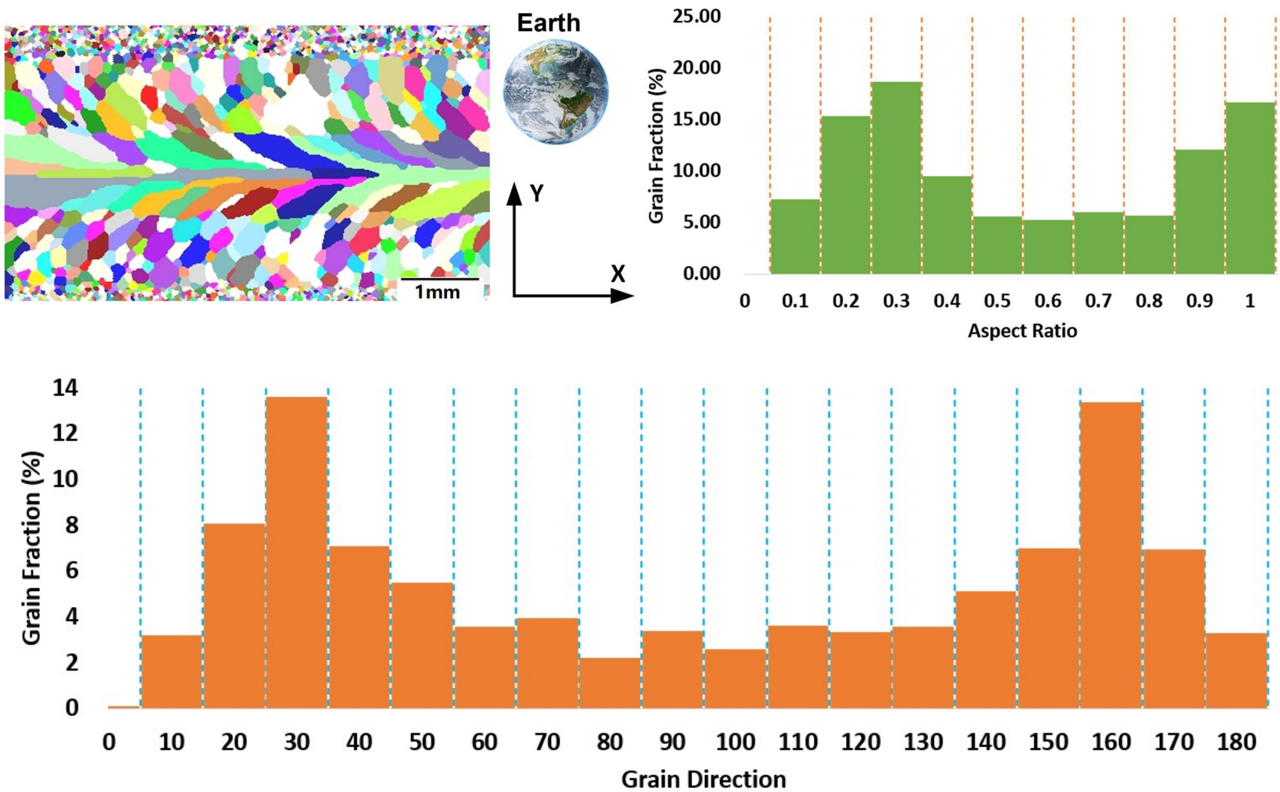
Earth
1mm
Y
X
Grain Fraction (%)
25.00
20.00
15.00
10.00
5.00
0.00
0 0.1 0.2 0.3 0.4 0.5 0.6 0.7 0.8 0.9 1
Aspect Ratio
14
12
10
8
6
4
2
0
0 10 20 30 40 50 60 70 80 90 100 110 120 130 140 150 160 170 180
Grain Direction

(a)

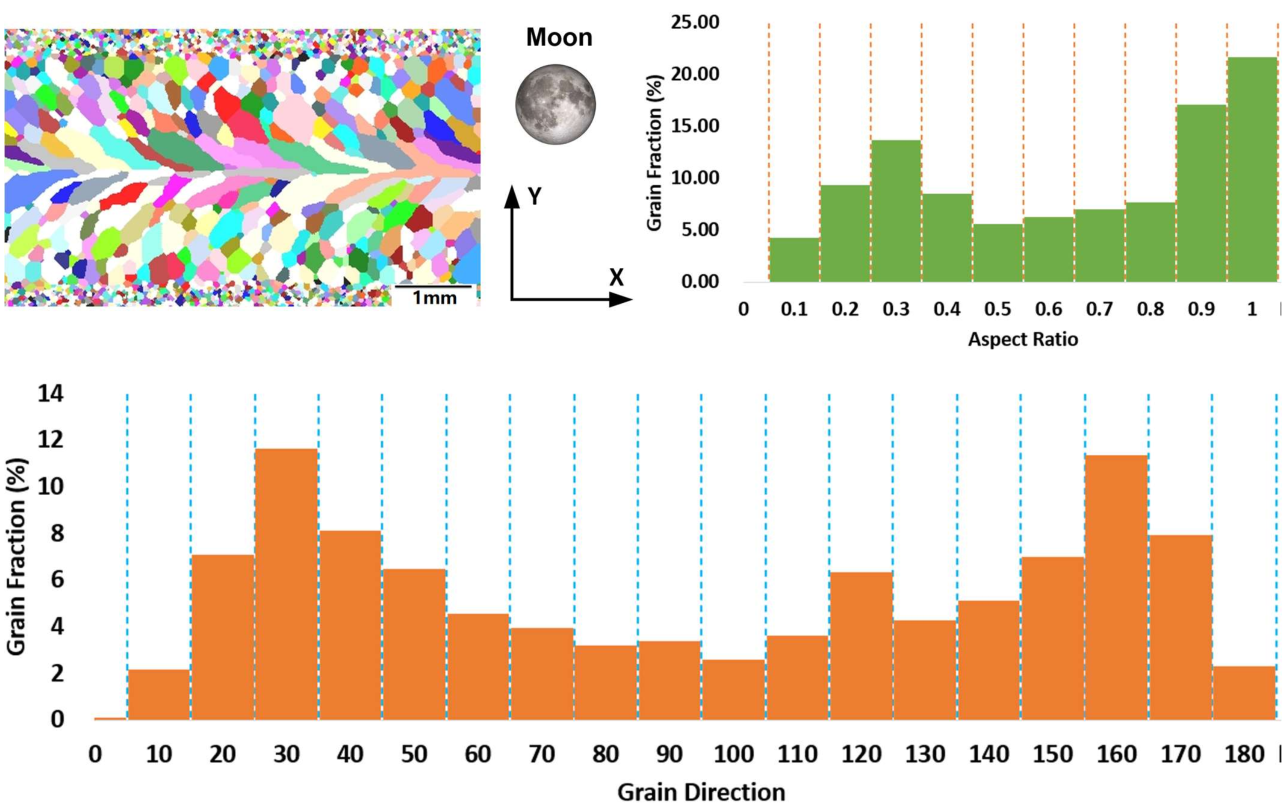
Moon
1mm
Y
X
Grain Fraction (%)
25.00
20.00
15.00
10.00
5.00
0.00
0 0.1 0.2 0.3 0.4 0.5 0.6 0.7 0.8 0.9 1
Aspect Ratio
14
12
10
8
6
4
2
0
0 10 20 30 40 50 60 70 80 90 100 110 120 130 140 150 160 170 180
Grain Direction

(b)

Figure 10. Grain aspect ratios and grain directions in the welding grain morphology simulated under (a) terrestrial and (b) lunar conditions.

In addition to the aspect ratio grain direction, grain size serves as a key quantitative indicator for assessing the influence of welding conditions on microstructural evolution. The results (Fig. 11) show that the average grain sizes are larger in terrestrial welding process by comparing with lunar welding process. These simulation results provide predictive insight that can be directly used to guide the adjustment of welding parameters across different gravity environments. By anticipating how molten pool evolution and grain size morphology respond to gravitational variation, the model enables informed parameter optimization for achieving targeted microstructures in both terrestrial and extraterrestrial welding conditions.

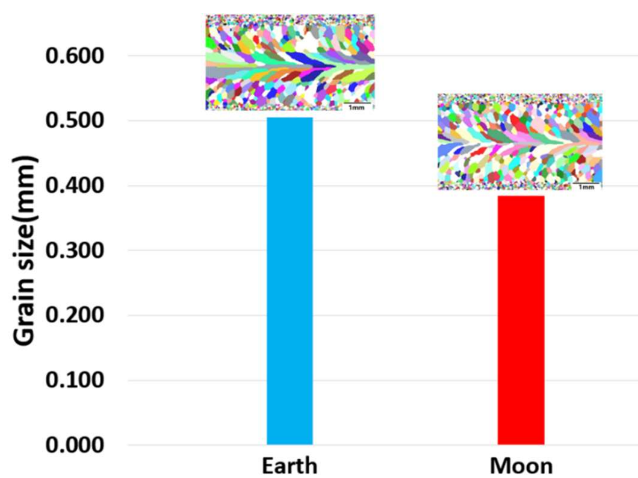

Figure 11. Grain-size comparison in the simulated welding grain morphology.

4.0 Conclusion

This work demonstrates the capability of the proposed hybrid modeling framework to simulate the coupled thermal and microstructural phenomena during the welding of Tantalum. First, the model successfully captures heat transfer, molten pool evolution, and grain growth at the weld joint, with its validity confirmed by the close agreement between simulated and experimentally observed grain morphologies. Second, the resulting weld microstructure is characterized by a coexistence of columnar and equiaxed grains. Columnar grains are concentrated near the molten pool, where directional solidification dominates, while equiaxed grains appear in regions farther from the fusion boundary. Finally, the orientation of columnar grains aligns primarily with the direction of molten pool movement, resulting in two preferred growth directions. These findings not only provide a deeper understanding of the welding process for Tantalum but also establish a predictive framework for tailoring weld microstructures in high-value refractory metals. Looking ahead, this hybrid simulation approach offers a powerful tool for designing welding processes in extreme environments, including space and lunar applications, where experimental validation is prohibitively costly or impractical.

5.0 Outlook

The hybrid simulation framework developed in this study enables the coupled prediction of thermal-fluid behavior and grain-scale microstructural evolution during metal welding under terrestrial conditions. Importantly, the model is not limited to terrestrial environments on Earth. By modifying key parameters such as ambient temperature, atmospheric pressure, and gravitational acceleration, the same framework can be adapted to simulate welding processes and grain growth on the surface of other planets or space stations within microgravity environments. This flexibility makes the approach particularly valuable for exploring welding strategies in extraterrestrial manufacturing scenarios. For example, by tailoring the boundary conditions to lunar surface conditions—characterized by high vacuum, low gravity, and extreme temperature fluctuations—the model can provide insights into molten pool dynamics, solidification behavior, and resulting microstructural morphologies. Such predictive capabilities offer a pathway toward developing reliable joining technologies for future space exploration and in-situ resource utilization on the Moon or beyond.

References

[1] Wei, H., T. Mukherjee, W. Zhang, J. Zuback, G. Knapp, A. De, T. DebRoy, "Mechanistic models for additive manufacturing of metallic components," *Progress in Materials Science*, 100703, 2020, 100703.

[2] Wu, Y.-C., C.-H. San, C.-H. Chang, H.-J. Lin, R. Marwan, S. Baba, W.-S. Hwang, "Numerical modeling of melt-pool behavior in selective laser melting with random powder distribution and experimental validation," *Journal of Materials Processing Technology* 254, 2018 72−78, 2018.

[3] Cheng, B., X. Li, C. Tuffile, A. Ilin, H. Willeck, U. Hartel, "Multi-physics modeling of single track scanning in selective laser melting: powder compaction effect," *29th Annual International Solid Freeform Fabrication Symposium—An Additive Manufacturing Conference*, 13−15, 2018.

[4] Hirt, C.W., B.D. Nichols, "Volume of fluid (VOF) method for the dynamics of free boundaries," *Journal of computational physics*, 39(1), 201−225.

[5] Holm, E.A., C.C. Battaile, "The computer simulation of microstructural evolution," *JOM*, 53(9), 2001 20−23, 2001.

[6] White, R.J., "The development of grain-face porosity in irradiated oxide fuel," *Journal of nuclear material,* 325(1), 61−77, 2004.

[7] Bishop, J.E.R., Theron, Kyle Johnson, Judith Alice, Brown, "Simulating the mechanical response of synthetic AM microstructures generated with Kinetic Monte Carlo techniques," 2016. https://www.osti.gov/biblio/1375297.

[8] Rodgers, T.M., J.D. Madison, V. Tikare, "Simulation of metal additive manufacturing microstructures using kinetic Monte Carlo," *Computational Materials Science,* 135, 78−89, 2017.

[9] Rodgers, T.M, J.D. Madison, V. Tikare, M.C. Maguire, "Predicting mesoscale microstructural evolution in electron beam welding," *JOM*, 68(5), 1419−1426, 2016.

[10] Rodgers, T.M., J.A. Mitchell, V. Tikare, "A Monte Carlo model for 3D grain evolution during welding, Modelling and Simulation in Materials Science and Engineering," 25(6), 064006, 2017.

[11] Wei, H., J. Elmer, T. DebRoy, "Three-dimensional modeling of grain structure evolution during welding of an aluminum alloy," *Acta Materialia*, 126, 413−425, 2017.

[12] Wei, H., J. Elmer, T. DebRoy, "Crystal growth during keyhole mode laser welding," *Acta Materialia,* 133, 10−20, 2017.

[13] H, Wei, G. Knapp, T. Mukherjee, T. DebRoy, "Three-dimensional grain growth during multi-layer printing of a nickel-based alloy Inconel," 718, *Additive Manufacturing,* 25, 448−459, 2019.

[14] Busch, G., M551 metals melting experiment, 1977.

[15] Ferreira, T., W. Rasband, *ImageJ user guide*, IJ, 2015.

[16] Li, W., M. Soshi, "Modeling analysis of the effect of laser transverse speed on grain morphology during directed energy deposition process," *The International Journal of Advanced Manufacturing Technology*, 103(9−12), 3279−3291, 2019.